# Bulk Purification and Deposition Methods for Selective Enrichment in High Aspect Ratio Single-Walled Carbon Nanotubes

Nidhi P. Bhatt, Pornnipa Vichchulada, and Marcus D. Lay*

Department of Chemistry and Nanoscale Science and Engineering Center (NanoSEC), University of Georgia, Athens Georgia, 30602

ABSTRACT: Aqueous batch processing methods for the concurrent purification of single-walled carbon nanotube (SWNT) soot and enrichment in high aspect ratio nanotubes are essential to their use in a wide variety of electronic, structural, and mechanical applications. This manuscript presents a new route to the bulk purification and enrichment of unbundled SWNTs having average lengths in excess of 2 μm. Iterative centrifugation cycles at low centripetal force not only removed amorphous C and catalyst nanoparticles but also allowed the enhanced buoyancy of surfactant encapsulated,

unbundled, high aspect ratio SWNTs to be used to isolate them in the supernatant. UV–vis–NIR and Raman spectroscopy were used to verify the removal of residual impurities from as-produced (AP-grade) arc discharge soot and the simultaneous enrichment in unbundled, undamaged, high aspect ratio SWNTs. The laminar flow deposition process (LFD) used to form two-dimensional networks of SWNTs prevented bundle formation during network growth. Additionally, it further enhanced the quality of deposits by taking advantage of the inverse relationship between the translational diffusion coefficient and length for suspended nanoparticles. This resulted in preferential deposition of pristine, unbundled, high aspect ratio SWNTs over residual impurities, as observed by Raman spectroscopy and atomic force microscopy (AFM).
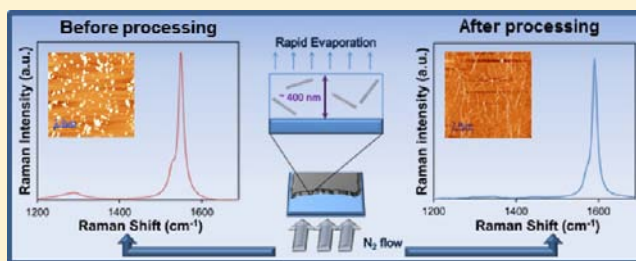
■ INTRODUCTION

Single-walled carbon nanotubes (SWNTs) have attracted great attention because of their unique electronic and mechanical properties. They have the highest measured tensile strength, are flexible, lightweight, and exhibit low power consumption while retaining high on/off ratios in electronic materials.[1] These seamless tubes of graphene are typically micrometers long and one nanometer in diameter. However, unlike graphene, SWNTs exist as either semiconductive or metallic conductors due to quantum confinement effects resulting from their curvature. Therefore, there is particular interest in using SWNTs for electronic applications. In spite of their great potential, the widespread use of SWNTs in electronic materials remains stalled by issues with unbundling and purifying them in order to obtain much greater precision over their electronic properties. This is critical as, regardless of the growth method, as-produced (AP) grade SWNT soot is a mixture of SWNTs (with bandgaps from 0 to ~1.8 eV), metal catalyst nano-particles, and amorphous carbon. Bulk processing methods for removing these impurities and unbundling SWNTs, without greatly increasing sidewall defects, is crucial to obtaining a fundamental understanding of the properties of individual SWNTs. Further, the fundamental electrical, optical, and electrochemical behavior of SWNT-based composites can be more reproducibly measured and understood if the suspensions from which they are deposited are well characterized.

Therefore, the development of scalable methods for incorporating SWNTs into a wide variety of structural and electron materials is strongly dependent on the creation of new liquid-processing techniques for purifying and separating nanotubes without damaging their enhanced physical attributes. However, significant issues remain with regard to forming suspensions of unbundled high aspect ratio SWNTs. These issues can be reduced to two broad challenge areas: (1) removing residual catalyst nanoparticles and amorphous C without damaging the SWNTs, and (2) forming suspensions of unbundled, high-aspect ratio SWNTs while maintaining control over the concentration and average length of the solvated nanotubes.

Addressing the first challenge area, the ability to form bulk quantities of suspensions composed of unbundled SWNTs having known average lengths is particularly important for forming and characterizing two-dimensional (2-D) SWNT networks that harness the enhanced electrical and physical properties of nanotubes.[2−4] In fact, many researchers are investigating the formation of SWNT-network based tran-sistors,[5−7] sensors,[8−10] and field-emission sources.[11,12] The electron mobility and on/off ratio of such materials are greatly hampered by residual impurities. Therefore, nonoxidizing purification methods will play a central role in SWNT-based electronics.

Methods of dealing with the second challenge area, forming suspensions of unbundled, high aspect ratio SWNTs, are also crucial to optimizing the performance of SWNT networks in electronic device structures. The electron mobility of SWNT networks decreases inversely with the number of SWNT–SWNT tunnel junctions. Therefore, maximizing the average

length of SWNTs in a network will decrease the number of inter-SWNT tunnel junctions that must be bridged. This will allow the low resistance and near ballistic electronic transport observed for unbundled SWNTs to be exploited.[13−15]

The charge carrier mobility for SWNT networks[16−18] has been reported to exceed two commonly used systems, amorphous Si[19−21] and organic semiconductors.[22,23] A recent study has even demonstrated electron mobility approaching those observed for p-type crystalline Si.[24] This performance advantage, coupled with the mechanical flexibility and transparent nature of SWNT networks,[25−27] as well as their ability to operate at low voltages, causes great interest for their use in portable electronic devices and displays. Furthermore, the tensile strength and heat conductance are greatly improved in polymer composites that contain cross-linked high aspect ratio SWNTs.[28,29] Therefore, bulk-processing methods for forming suspensions enriched in unbundled, undamaged, high aspect ratio SWNTs will play a central role in the development of a wide variety of electronic and structural materials.

Understanding bulk solution processing methods is crucial to the deposition of SWNT networks on heat-sensitive substrates used in flexible electronic materials, as direct growth of nanotubes (which requires temperatures in excess of 700 °C) is not possible. For these reasons, the recent literature is replete with reports of suspension purification and processing methods, which often begin with oxidative purification treatments.[30−33] Yet, oxidation reduces the electrical conductivity of SWNTs through the introduction of sidewall defects.[8,9] Following oxidation, other suspension processing methods include density gradient ultracentrifugation (DGU),[34−37] and polymer wrapping.[38] While DGU has been shown to be useful for separating SWNTs on the basis of diameter and type of conductivity, its major disadvantage is that it yields nanotubes with lengths only up to a few hundred nanometers, as it employs centripetal forces in excess of 100,000g. Additionally, DGU and polymer wrapping involve the use of reagents that are difficult to remove, a requirement for electronic applications. In particular, DGU involves the use of several surfactants, as well as a density gradient medium, typically iodixanol. This compound binds strongly to SWNTs and requires a separate dialysis treatment for removal.

Therefore, while effective at reducing residual metal catalysts, the concurrent oxidation of SWNTs and the formation of highly carboxylated carbonaceous impurities which are difficult to remove are significant concerns.[33] This group has recently demonstrated that purification through iterative low g centrifugation cycles is effective at removing residual metal catalyst and carboxylated carbonaceous impurities, without increasing the density of defects observed for SWNTs.[39−41] This manuscript describes how this benign purification method can be used to produce stable suspensions of SWNTs having lengths in excess of 2 μm. This group is currently investigating methods of further separating these high aspect ratio nanotubes by diameter and type of conductivity.

This report provides insight into the separation of unbundled, surfactant encapsulated, high-aspect ratio SWNTs from impurities under relatively low centripetal force (18,000g), and demonstrates a great improvement in the quality of deposits that can be formed. Repeated centrifugation/decantation is shown to enrich suspensions in unbundled high aspect ratio SWNTs. The hydrophobic nature of SWNTs necessitates the use of an emulsifier to support SWNT dispersion. Various species, including surfactants, DNA, polymers, and lipids, can

be used to this effect. Surfactants are commonly used if the ultimate goal involves formation of electronic materials, since they can be more easily removed after the nanotubes are deposited. Of the various surfactants available, sodium dodecyl sulfate (SDS) was chosen for these studies because it has the lowest binding energy with SWNTs of the average diameter ($\sim$1.55 $\pm$ 0.1 nm) observed for the arc discharge soot used in these studies.[42] This is an important consideration, as the ultimate goal is to remove the surfactant after deposition of the SWNTs, in order to improve electronic performance and reproducibility.[43]

Recently published work by this group concerned the use of chemical and heat treatments that are compatible with heat-sensitive substrates to improve the resistance and interdevice precision of networks that were cast from SDS suspensions.[44] When several highly resistive networks of similar SWNT densities were treated with mild oxidative and annealing treatments, a 13-fold reduction in resistance was accompanied by a 28-fold increase in internetwork precision. The effectiveness of this treatment for increasing conductivity by removing SDS was verified by Raman microscopy. Additionally, the increase in conductivity and precision was also ascribed to the formation of "molecular anchors," which served to decrease the tunnel barrier at junctions between SWNTs.

Although many commonly reported purification methods have the potential to address either of the two challenge areas listed earlier, the approach described in this manuscript concurrently addresses both challenges by achieving (1) purification of SWNT soot without damaging oxidative treatments, and (2) the formation of stable suspensions of unbundled, high aspect ratio SWNTs having controlled concentration and length. Raman spectroscopy and UV−vis−NIR spectroscopy are used to confirm that impurities are removed by each purification cycle, while SWNTs remain suspended. Atomic force microscopy (AFM) demonstrates the effectiveness of this purification method for the formation of SWNT deposits in on Si/SiO$_x$ wafer fragments.

The laminar flow deposition method developed by this group ensures that nanotube bundling does not occur during the deposition process.[45−47] It has been shown to allow great control over the density and alignment of unbundled SWNTs deposited on self-assembled monolayer-modified surfaces.[47] This deposition method is a critical part of these studies, as the ability of the suspension processing method to remove SWNT bundles can only be ascertained by AFM if bundle formation is prohibited during the deposition process. This group's deposition method is also an important new tool in SWNT network formation, as other common deposition methods, such as layer-by-layer,[48] fluidic assembly,[49] and dip-coating[50] result in bundles of SWNTs.

■ EXPERIMENTAL DETAILS

Formation and Purification of SWNT Suspensions. To form the suspensions, 1 mg/mL AP grade arc discharge soot (Carbon Solutions, Inc.) was dispersed in 1% SDS (J.T. Baker) solution via 30 min of probe ultrasonication (Fisher model 500) at a power density of 0.4 W/mL, which imparted 21 kJ of energy to the suspension. Previous work by Vichchulada et al. has demonstrated that these conditions are optimum for the production of suspensions of unbundled SWNTs while minimizing sonication-induced damage to the SWNTs.[51] Next, SWNT suspensions were distributed into 1.5 mL centrifuge tubes and centrifuged (Beckman Microfuge) for either 45 or 90 min at 18,000g, as described in Figure 1a. After centrifugation, the supernatant was carefully removed in 0.2 mL aliquots, labeled A, B, C, D, and E.

9353

dx.doi.org/10.1021/ja302136x | *J. Am. Chem. Soc.* 2012, 134, 9352−9361
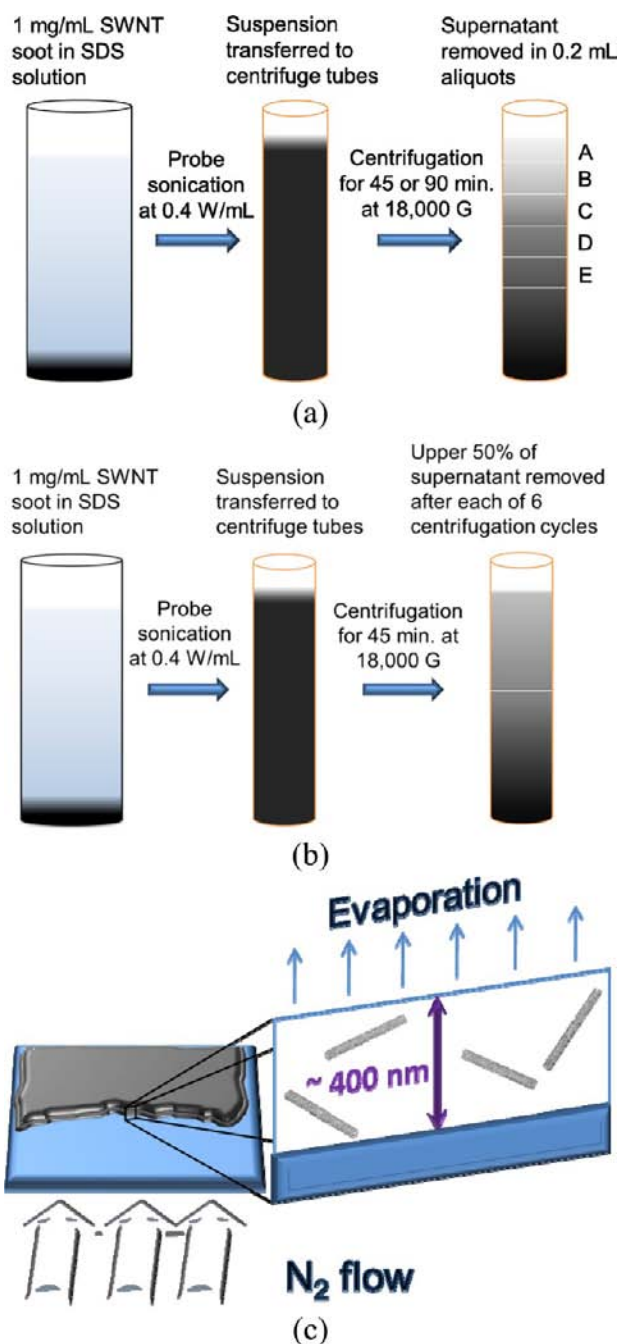
Figure 1. Schematic for the two experimental approaches employed (not to scale). Probe sonication at a power density of 0.4 W/mL was used to form suspensions of AP-grade SWNT. Then, the suspensions were either (a) treated with centrifugation at 18,000*g* for 45 or 90 min, followed by careful removal of the supernatant in 0.20 mL aliquots; (b) the upper 50% of the supernatant was carefully removed after each of six 45 min centrifugation cycles; or (c) since the importance of shear forces is supplanted by viscous forces as the suspension thins, low densities of unbundled SWNTs were isolated and deposited via rapid evaporation, without the possibility of bundle formation. This allows the degree of SWNT bundling in the processed suspension to be assessed.

Spectroscopic and scanning probe data were obtained for each of these aliquots.

In order to determine the effect of multiple centrifugation cycles on the purity and enrichment in high aspect ratio SWNTs, the upper 50% of the supernatant was carefully collected after each of six 45 min

centrifugation cycles (Figure 1b). Then, the upper fractions were placed in new centrifuge tubes, and the process was repeated. This allowed observation of the effect of iterative processing steps on the purity and average length of SWNT suspensions and deposits.

Formation of SWNT Deposits via Laminar Flow Deposition (LFD). Si/SiO$_x$ wafers were cut into 1×1.5 cm fragments and cleaned with compressed CO$_2$. Prior to SWNT deposition, the substrates were modified with a self-assembled monolayer by a 45 min immersion in a solution of 2.11 mg/mL 3-aminopropyl triethoxysilane (99%, Sigma Aldrich) in ethanol (99.5%, absolute 200 proof, ACROS). In order to ensure that only one monolayer of the silane remained, the substrates were washed with copious amounts of ethanol and water. Then they were dried in a stream of N$_2$ gas. Finally, they were cleaned with compressed CO$_2$, as this has been demonstrated to remove excess layers of polymerized silane.[52]

After substrate preparation, two deposition cycles, each using 90 μL of SWNT suspension, were used to form the low-density SWNT deposits that would be used for AFM analysis. Each deposition cycle consisted of wetting the silane-coated Si/SiO$_x$ wafer with the SWNT suspension, followed by quick drying in a stream of N$_2$ gas at a pressure of 60 psi (Figure 1c). The wafers were then rinsed with copious amounts of nanopure water (>18.1 MΩ) and then dried again under a stream of N$_2$ gas.

In this manner, bundle formation was prohibited during the drying process by greatly reducing the height of the suspension to a thin layer (∼400 nm in thickness) that was characterized by viscous flow, prior to nanotube deposition, as described by Zhang et al.[45] Because the translational diffusion of these isolated SWNTs was quite low, they were deposited on the surface in low densities during a brief evaporation phase. Therefore, this deposition method facilitated the deposition of individual SWNTs, as long as they were unbundled in the processed suspension.

Characterization of SWNT Suspensions and Deposits by UV−vis−NIR Spectroscopy, AFM, and Raman Spectroscopy. UV−vis−NIR spectroscopy (Cary, 5000) was performed using a quartz cell with a path length of 1 mm. An absorbance of 600 nm has been found to yield a linear relationship between SWNT concentration and absorbance.[53] This is likely due to the lower scattering efficiency of SWNTs at this wavelength and the fact that it falls between absorbance bands for semiconductive and metallic SWNTs. However, carbonaceous impurities have a maximum absorbance ∼242 nm;[54] thus, comparison of the data obtained for these two wavelengths was used to quantitate the purity of the suspensions during processing.

AFM images were obtained via intermittent contact mode in air (Molecular Imaging, Pico Plus). Five areas of each sample were analyzed with AFM image analysis software (WSxM, v 5.0)[55] to determine the effect of the separation process on the average height, and length of SWNTs, as well as the surface height and roughness. This provided information on the concentration of bundles and the degree of length separation obtained. Additionally, the change in surface height and roughness was also evaluated in order to determine the density of residual impurities.

Raman spectroscopy (Thermo Scientific, DXR SmartRaman) was performed on suspensions in a sealed capillary tube and on SWNT deposits without any further modification. A charge-coupled device (CCD) detector was used to record spectra obtained using a 532 nm diode laser excitation source. Suspensions were analyzed with a 10× objective and a source intensity of 10 mW at the sample, while for SWNT deposits, a 50× objective with 1 mW intensity at the sample was employed.

■ RESULTS AND DISCUSSION

Effect of Processing Time on the Purification of SWNT Soot. For both 45 and 90 min processing times, the magnitude of the UV−vis-NIR absorbance for each suspension increased in alphabetical order with each aliquot (Figure 2), indicating the presence of a density gradient in carbonaceous impurities. By comparison, the data for 45 min had a higher absorbance for
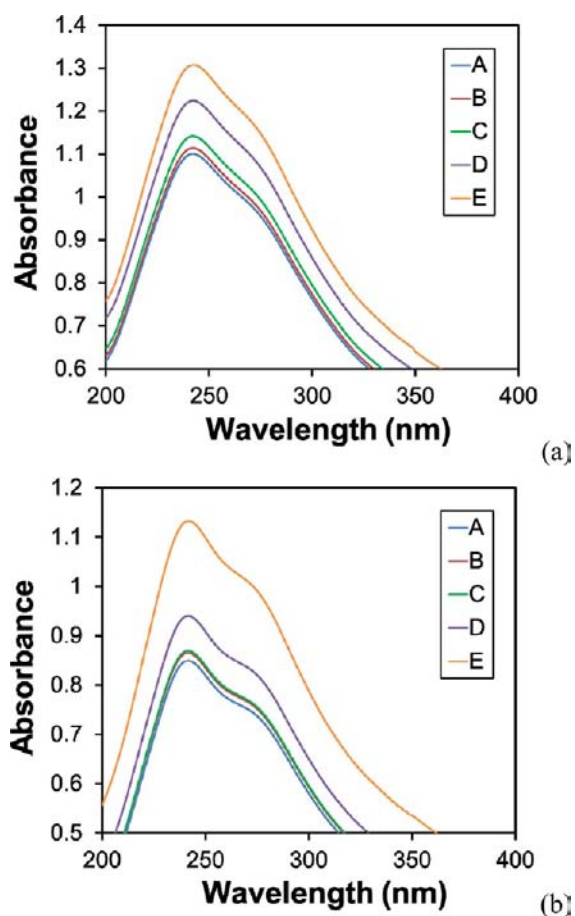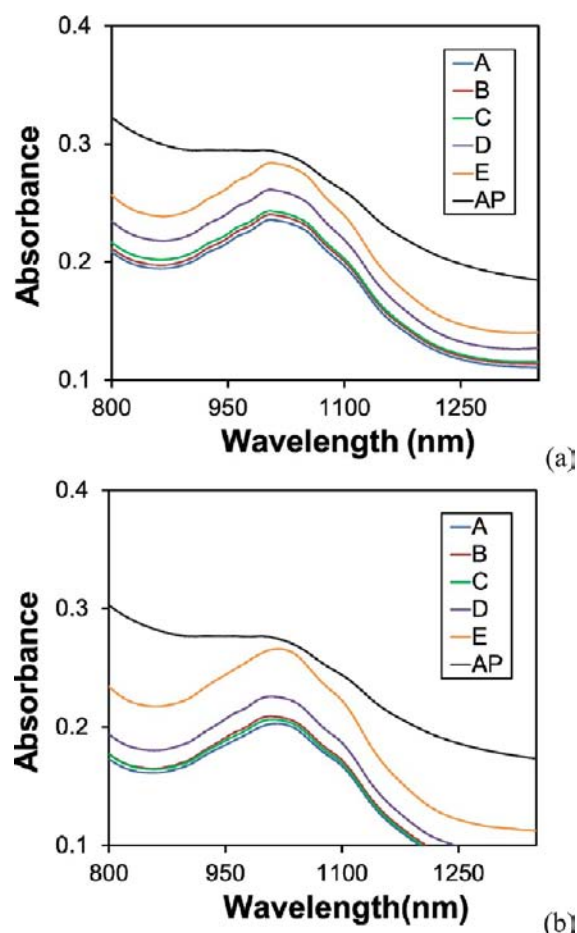
Figure 2. Absorbance in the UV region of the spectra for aliquots A–E increased from the top to the bottom for both processing times; (a) after one 45-min step, the shoulder on the low energy side of the band at 242 nm was less pronounced than (b) after processing at 90 min.

Figure 3. For NIR spectra of the E_{22} transitions for semiconducting SWNTs, the unprocessed suspension was normalized to the peak ~1010 for sample E and then offset by 0.1 absorbance units for clarity. (a) After 45 min of processing, a greater absorbance, and presence of fine structure, was observed on the high-energy side of the band, while (b) for 90 min, the absorbance was lower and a greater difference in the magnitude of the absorbance was observed between aliquots corresponding to the line between the upper and lower 50% of the suspension (between aliquots labeled D and E).

every layer, relative to its counterpart in the 90 min data. Additionally, aliquots A for both samples had the lowest peak absorbance at ~242 nm, with values of 1.11 and 0.86 for 45 and 90 min, respectively. Aliquots B and C were relatively close to A in magnitude, but there was a significant increase in absorbance for D and E. As each aliquot represented 0.2 mL of suspension, this indicated that after both processing procedures, the upper 50% of the supernatant was significantly improved in purity.

Aliquot E consistently had the greatest absorbance for all samples, achieving a peak absorbance of 1.31 and 1.13 for 45 and 90 min, respectively. This greater absorbance indicates that 90 min is more effective at isolating the amorphous carboxylated C impurities and SWNT bundles in the lower half of the centrifuge tube. Therefore, a large portion of the impurities in the SWNT soot was sequestered in the lower 50% of the sample, culminating in a pellet at the bottom. The shoulder at ~275 nm, on the low-energy side of the peak, became more pronounced at longer centrifugation times. This is due to the high extinction coefficient for amorphous C impurities.[56,57]

In the region of the spectra that corresponds to the second interband transitions (E_{22}) for semiconducting SWNTs, ~1010 nm, the absorbance decreased significantly after processing at either 45 or 90 min. (Figure 3). As the average absorbance observed for unprocessed suspensions was 2.14, it was normalized to the absorbance for aliquot E and offset by 0.1

absorbance units to allow visualization of the change in the size of the peak before and after processing. This significant reduction in absorbance between AP-grade and processed suspensions was expected, due to the significant reduction in residual carbonaceous impurities, which increased the baseline of the absorbance of the suspensions throughout the visible and NIR range and bundles of SWNTs.

The increased size of the semiconducting interband transition peak relative to the baseline is indicative of the enrichment of the suspension in unbundled SWNTs, as the absorbance due to these transitions is not quenched, as in bundled SWNTs. Also of note in the NIR spectra is the presence of small waves on the low-wavelength side of the band centered at 1010 nm. These peaks are indicative of electronic transitions in SWNTs of various chirality and diameters.[58] These peaks are better resolved in suspensions of short nanotubes.

Evidently, the viscosity of the aqueous solvent used in these studies was sufficient to stabilize the density gradients such that they could be observed in each aliquot, without the need for a density gradient in the solvent. This is consistent with a recent

report of a NIR fluorescence videomicroscopy study that determined the translational diffusion coefficient for un-bundled, surfactant-encapsulated SWNTs may range from 0.3 to 6 μm^2/s, with high aspect ratio SWNTs at the lower end of this range.[59] Short SWNTs, down to 130 nm, were observed to have the highest translational diffusion coefficients while those of ~1 μm in length had the lowest coefficients.

The absorbance at 242 nm is sensitive to π electron-containing amorphous carbon impurities, as well as the plasmon resonances in the free-electron clouds of the nanotubes. The measured absorbance in this range is also augmented by scattering that occurs when short wavelength light interacts with suspensions of carbon nanotubes.[53] The absorbance at 600 nm is more sensitive to the SWNTs. This allows a qualitative estimate of the degree of purification, because a decrease in the magnitude of the ratio $A(242\ nm)/A(600\ nm)$ indicates a decrease in the absorbance of carbonaceous impurities, relative to that for SWNTs (Figure 4). Across processing times, 90 min was found to yield slightly
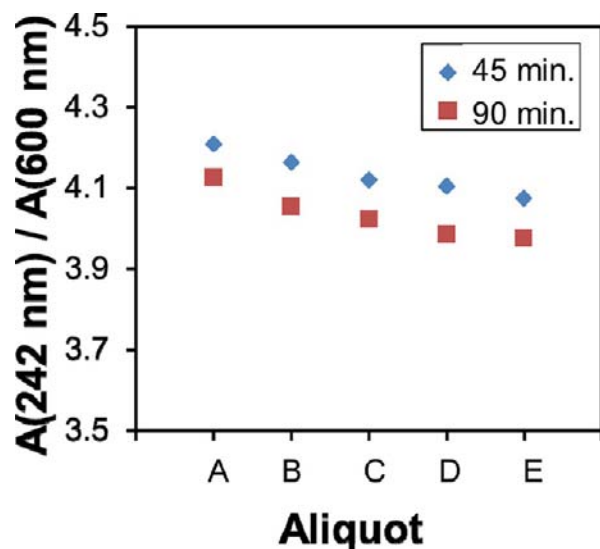
Figure 4. Due to the high extinction coefficient of impurities at 242 nm, relative to that of SWNTs at 600 nm, the ratio of the absorbance at these two wavelengths is indicative of changes in the purity and concentration of SWNT after each processing step. The slighter lower ratios for 90 min processing periods indicate a slight increase in the ability to remove impurities.

lower ratios. This is likely due to the greater processing time facilitating the removal of more impurities. AFM analysis, discussed in a subsequent section, corroborates this assertion.

Raman spectroscopy is well suited for characterizing the relative purity of SWNT suspensions and deposits due to the high Raman scattering efficiency of both defect-free and disordered sp^2 hybridized carbon atoms. The graphite band (G-band), which occurs near 1590 cm^{-1}, is indicative of tangential phonons in the pristine nanotubes, while the disorder band (D-band), near 1370 cm^{-1}, is indicative of asymmetric stretching in amorphous sp^2 hybridized C (Figure 5 shows Raman data for suspensions and deposits after 90 min processing). When the Raman spectra are normalized to the intensity of the G-band for each processing time, the ratio of the two intensities (I_G/I_D) is a measure of the relative enrichment of pristine SWNTs and removal of amorphous C impurities.
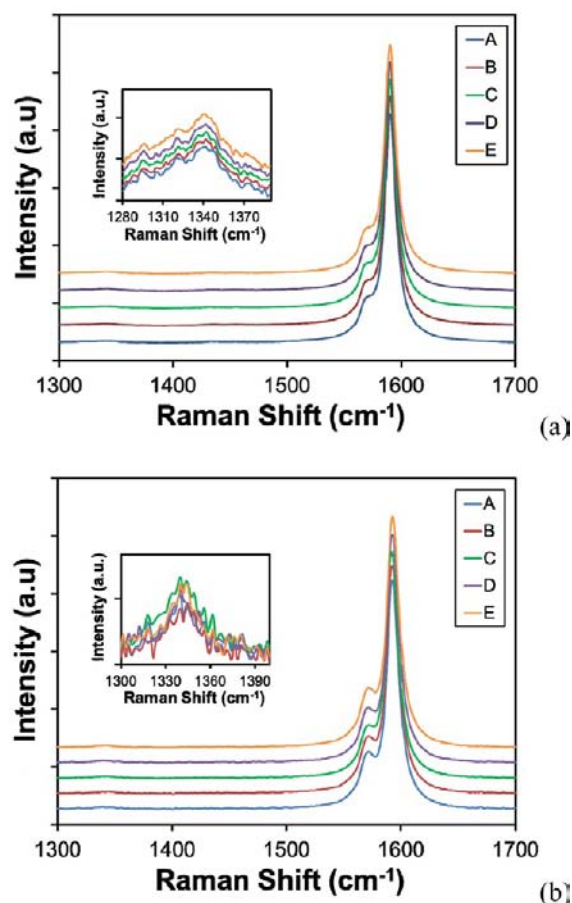
Figure 5. Representative Raman spectra obtained after 90 min processing periods for: (a) SWNT suspensions and (b) deposits. Insets show the D-band regions.

For both processing times, liquid Raman experiments exhibited a small trend toward lower I_G/I_D ratios for each aliquot (Figure 6). Yet, there was a pronounced difference between the I_G/I_D ratios obtained for suspensions vs deposits. The I_G/I_D ratio for suspensions increased by more than 100% with increased processing time; the ratio for deposits formed from those suspensions increased by only 15%. This indicates that the LFD process is another manner by which the impurities are removed.

Effect of Processing Time on the Enrichment in High Aspect Ratio SWNTs. AFM is indispensable in the study of purification and enrichment of SWNT soot as it allows a direct correlation between the suspension processing method and the qualities of the SWNT networks that can be formed. For both processing times, aliquot A was observed to have a higher density of SWNTs and globular impurities, with the density of impurities increasing in ascending order (Figure 7). For 45 min processing times, the average length of SWNTs decreased from 1.45 ± 0.4 to 0.9 ± 0.2 μm between aliquots A and E, wherease for 90 min, the lengths decreased from 1.75 ± 0.4 to 0.85 ± 0.2 μm. This indicated that just one processing step was sufficient to begin the process of enriching the supernatant in high aspect ratio SWNTs, although significant impurities remained.

For both processing times, the suspended high aspect ratio SWNTs remained stable in the supernatant for periods that allowed removal of each aliquot. AFM analysis indicated average lengths between 1.2 and 2.0 μm. In order to determine the purity of each deposit, a histogram was plotted for the
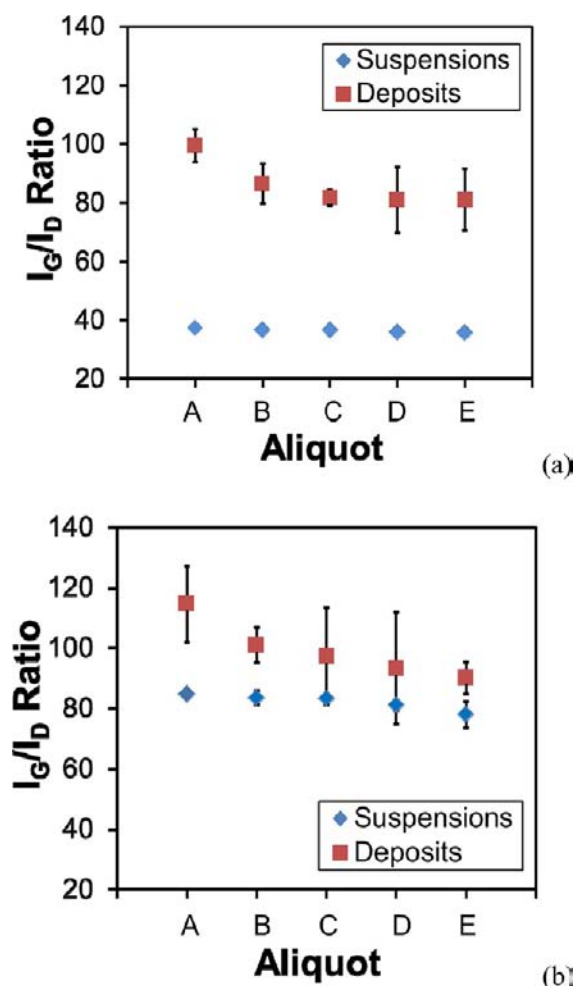
Figure 6. Average I_G/I_D ratios observed for SWNT suspensions and deposits formed from each aliquot showed an overall decrease in magnitude with ascending order. A difference in the ratios for suspensions and deposits was observed to be greater for (a) 45 min than for (b) 90 min, indicating that the LFD method used to form the deposits preferentially deposited high aspect ratio SWNTs over residual impurities in the suspension processed for 45 min.

height, or z-range data for each AFM image. This allowed quantitation of the average height, and thus level of impurities on the surface, since arc discharge nanotubes have an average height of 1.55 ± 0.1 nm, while impurities are generally much larger. There was a consistent trend toward a higher average height with ascending order for each aliquots, with the average height increasing from 7.98 to 34.87 nm for suspensions processed for 45 min, and from 10.48 to 13.05 nm for 90 min. Therefore, 45 min periods resulted in better quality deposits formed from the upper levels of the supernatant.

Within each sample, the rms surface roughness also increased in alphabetical order within each sample, while across processing times, the rms roughness increased at a faster rate for the samples processed for the shorter period (Figure 8). The roughness values increased from 3.09 to 7.29 nm, and from 3.51 to 5.02 nm for 45 and 90 min, respectively. This indicates that the shorter processing period allowed sufficient time for separation of impurities but was less effective at pelletization of impurities. The consistent increase in the observance of impurities with each aliquot indicates the stability of the suspensions with regard to the impurities that were sequestered

near the bottom of the centrifuge tube during processing. This represents a significant advance in the separation of SWNTs from impurities, and enrichment in high aspect ratio nanotubes, as this level of separation was achieved without requiring the addition of the density gradient media such as iodixanol, commonly used in DGU. This reagent is much more difficult than SDS to remove after an SWNT deposit is formed, as described in recent reports.[60,61]

Effect of Iterative Processing on the Separation of High Aspect Ratio SWNTs. AFM analysis showed that processing periods of 45 min not only yielded the highest density of high aspect ratio SWNTs but also resulted in deposits that had significant residual impurities. Therefore, an iterative approach (Figure 1b) was used in order to determine the efficacy of this processing method for producing suspensions enriched in longer SWNTs, while also achieving a greater degree of purity in deposits. For these suspensions, the ratio $A(242 \text{ nm})/A(600 \text{ nm})$ exhibited a slight increase with each processing step (Figure 9). This indicates that although both absorbances decreased with each processing iteration, $A(600 \text{ nm})$ was decreasing at a faster rate relative to $A(242 \text{ nm})$, causing a slight increase in the ratio of the absorbances from processing iteration 1 to 6. This is consistent with previous work from this group that shows that most of the globular impurities were removed in the first processing step.[41] Therefore, each successive processing step refined the suspension by removing small bundles of SWNTs, as well as residual carbonaceous impurities. Since $A(242 \text{ nm})$ is sensitive to both impurities and the free-electron clouds in the SWNTs, the loss of these bundles caused $A(600 \text{ nm})$ to decrease at a faster rate than $A(242 \text{ nm})$, resulting in a slight increase in the ratio $A(242 \text{ nm})/A(600 \text{ nm})$.

AFM images of unprocessed samples exhibited a high coverage of large globular impurities and large SWNT bundles (Figure 10). However, a dramatic improvement in the quality of the deposit can be seen after the first processing step, as most of the large impurities were removed as discussed previously. After the sixth iteration, the highest density of SWNTs, relative to that of impurities, was observed. Semiconductive 2-D networks of SWNTs, for electronic materials applications, can be readily formed from suspensions of this quality by increasing the number of deposition cycles until the percolation threshold for semiconductive nanotubes is exceeded.

The average height was observed to decrease from 40.00 to 1.31 nm (Table 1). This final height, which is consistent with the height of one SWNT, indicates a significant improvement over previous reports of the deposition of SWNTs. With each processing step, there was also a steady decrease in the average height and root mean square (rms) roughness values, indicating that the few impurities that remained were significantly smaller than in the unprocessed sample. Importantly, there was a concurrent increase in the average length of SWNTs from 1.18 to 2.07 μm, indicating that each iteration further enriched the supernatant in high aspect ratio SWNTs, while removing shorter nanotube fragments with other impurities.

Of great significance is the fact that the average density of SWNTs in each deposit increased from 0.31 to 0.79 SWNTs/ μm^2, further indicating the continued enrichment of high aspect SWNTs in the supernatant with each processing step. This can be explained by the increased buoyancy of longer SWNTs in these aqueous suspensions. Nair et al. observed that the buoyancy of a surfactant-encapsulated SWNT increases with
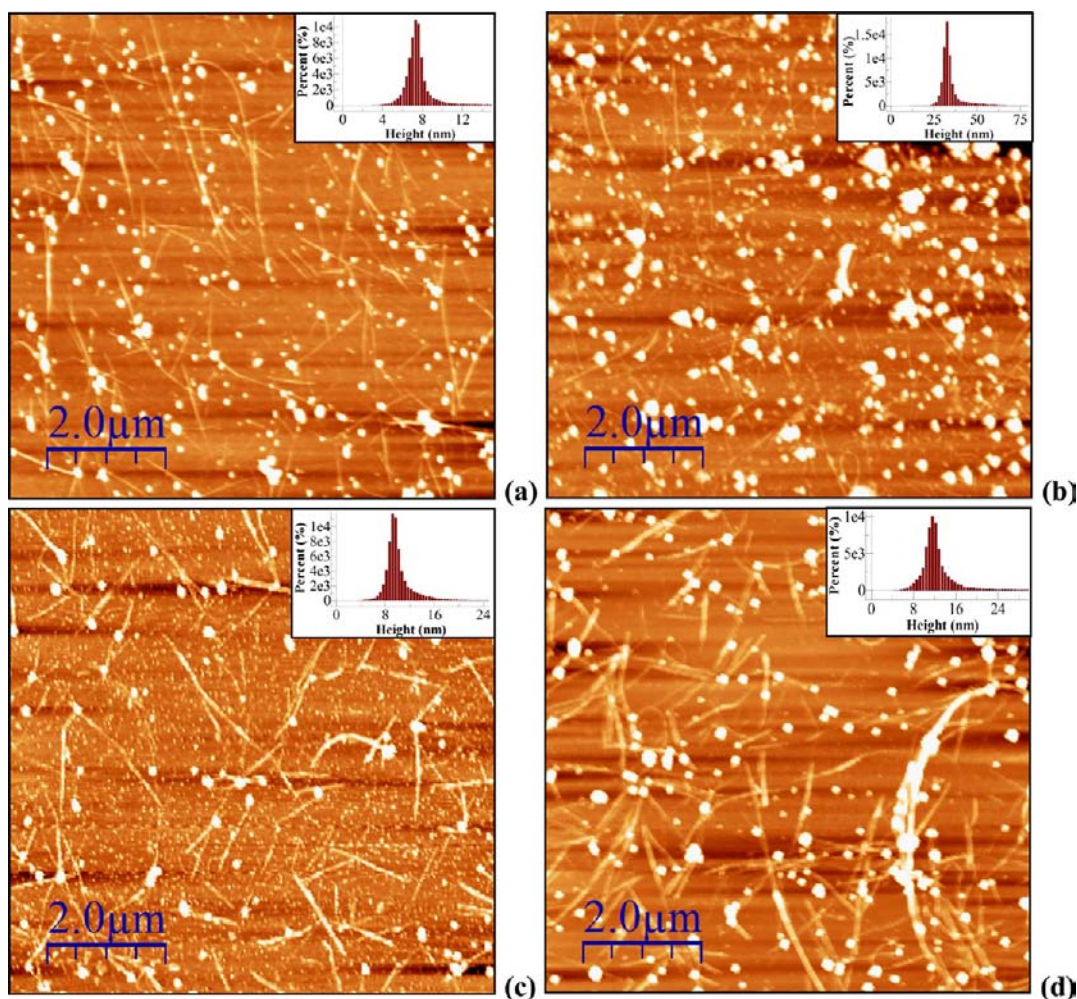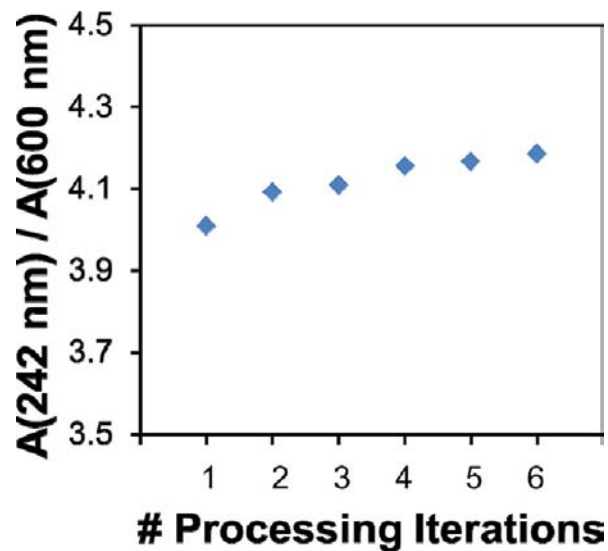
Figure 7. AFM images ($8 \times 8 \ \mu$m) for SWNT deposits on Si/SO$_x$ wafer fragments showed that 45 min processing times led to a density of SWNTs and impurities between aliquots A and E (a,b), respectively, greater than 90 min periods for aliquots A and E (c,d), respectively.
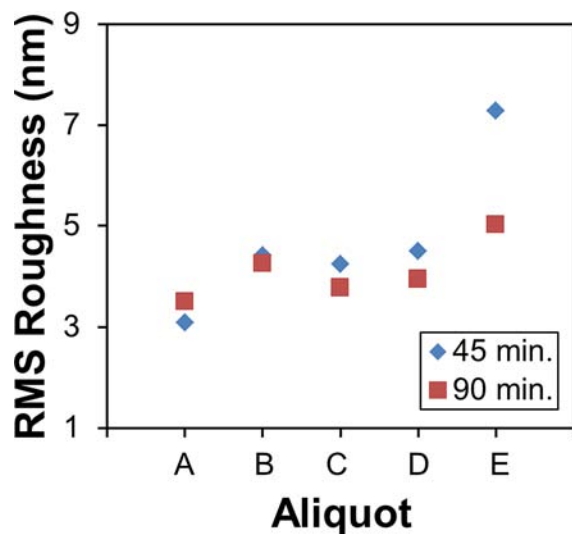

Figure 8. Rms roughness values for 45 and 90 min processing times were in close agreement for the first few aliquots. However, at lower levels of the suspensions, the shorter time for separation and pelletization of impurities resulted in increased surface roughness.

Figure 9. Ratio of A(242 nm)/A(600 nm) was highest for an AP suspension of 0.1 mg/mL SWNT soot. A sudden drop in the ratio after the first processing step indicated that much of the carbonaceous impurities were removed in the first processing step. Then, the increase in this ratio with each processing step indicated enrichment in unbundled SWNTs.

the density of surfactant molecules adsorbed along the nanotube length for various surfactants and chiralities.[62] In

9358

dx.doi.org/10.1021/ja302136x | *J. Am. Chem. Soc.* 2012, 134, 9352−9361
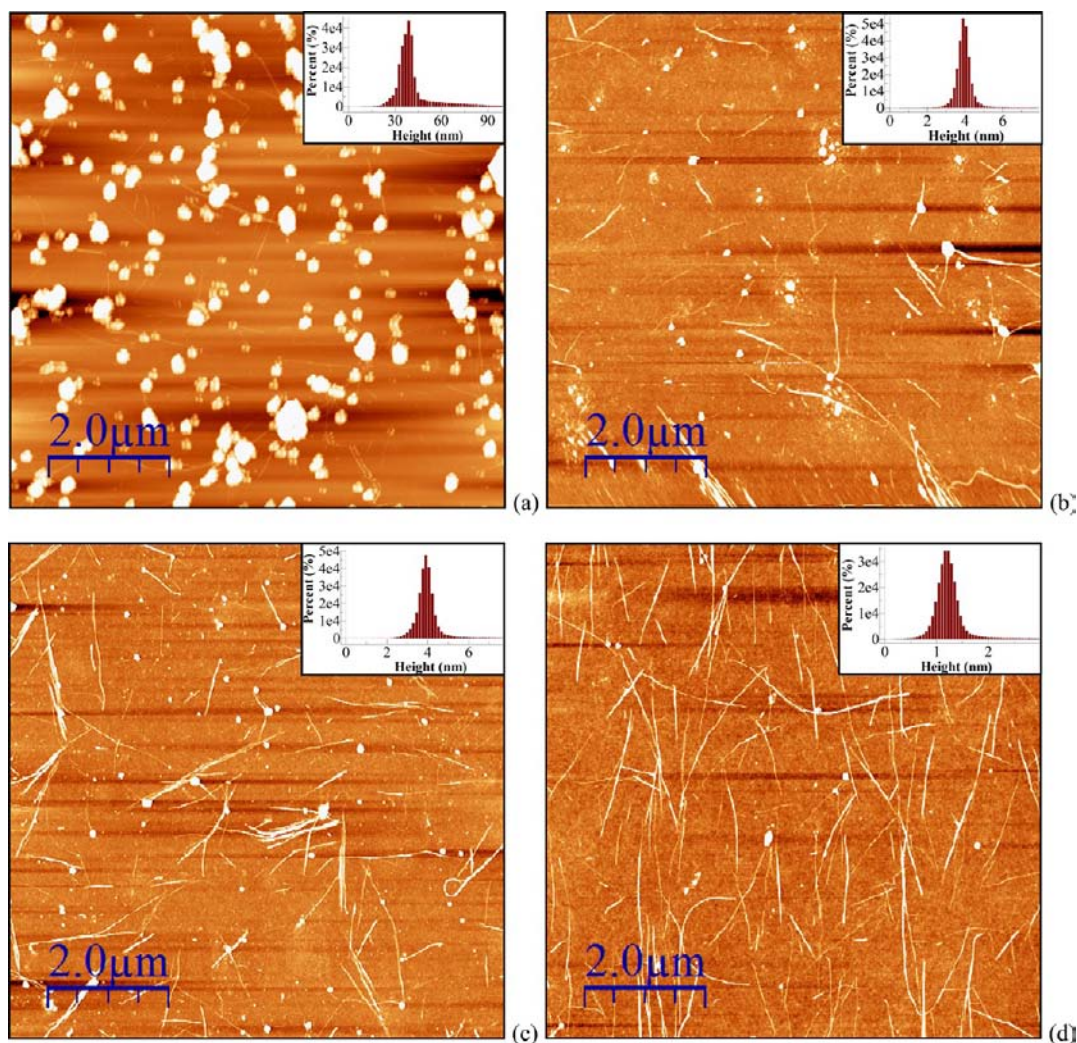
Figure 10. Representative AFM images (8 μm × 8 μm) for deposits formed from suspensions at various stages of processing; (a) an unprocessed suspension resulted in a deposit with average height of 40.00 nm; (b) the average height decreased to 4.89 nm after the first processing iteration; (c) after three steps, the average height was 3.38 nm; (d) six stages resulted in an average height of 1.31 nm, indicating significant removal of impurities and unbundling of SWNTs.

**Table 1. AFM Analysis of the Effect of Iterative Processing Steps on Low-Density SWNT Deposits**

# Processing iterations	AP	1	2	3	4	5	6
# SWNTs/μm^2	-	0.31	0.42	0.48	0.54	0.59	0.79
Average Length (μm)	-	1.18	1.31	1.55	1.65	1.70	2.07
% Standard Deviation	-	10	17	12	15	8	11
Average Surface Height (nm)	40.00	4.89	4.67	3.38	3.18	3.48	1.31
RMS Surface Roughness (nm)	13.7	1.91	1.89	1.54	1.39	1.31	1.21

addition, recent work has indicated that SDS molecules orient perpendicular to the hydrophobic sidewalls of suspended SWNTs. This increases the volume while decreasing the density of the SDS/SWNT construct.[63] Therefore, in this work, these unbundled, high aspect ratio SWNTs provide more area for the adsorption of SDS, increasing their relative buoyancy. Then, the low centripetal forces used in these studies not only remove low aspect ratio impurities but also allow the enhanced buoyancy of unbundled high aspect ratio surfactant-encapsulated SWNTs to isolate them in the supernatant.

The LFD Method Results in Further Purified Deposits.
The I_G/I_D ratios calculated from Raman spectra of suspensions and deposits indicated an increase in the quality of the deposit relative to that of the suspension, as determined from the increased signal for pristine sp^2-hybridized C, relative to defect-containing allotropes (Figure 11). This increase in I_G/I_D ratio with increasing processing iterations is due to the enrichment of the suspensions in high aspect ratio SWNTs with pristine sidewalls, as well as the removal of amorphous carbon. For suspensions, the I_G/I_D ratios increased by roughly a factor of 3 over the course of the first two processing iterations. However, there was a factor of 4 increase for deposits over this same range, indicating that the LFD network formation step is an additional purification step in the formation of thin films, providing the suspension has been purified of the more dense particulates. The formation of deposits of high aspect ratio SWNTs is further facilitated by the greater translational diffusion coefficient for shorter SWNTs making it more likely that they remain in suspension during the deposition process. Therefore, the increase in the ratio for deposits relative to that observed for suspensions is also due to the decreased presence of short SWNTs that likely have oxidized ends.
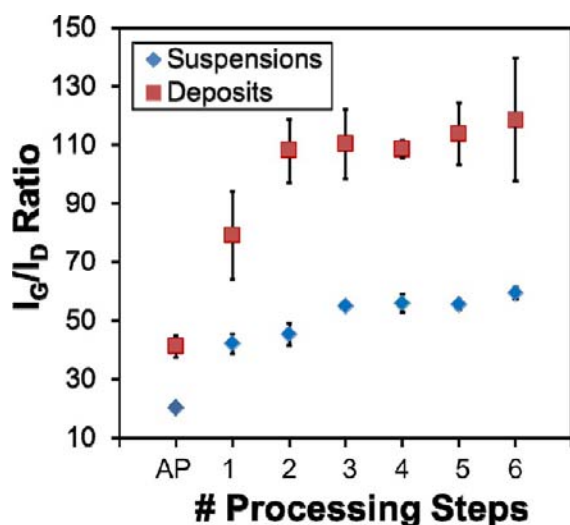
Figure 11. Evolution of Raman I_G/I_D ratios for suspensions and deposits of SWNTs over six processing iterations shows that the deposition process plays an important role in separating pristine SWNTs from impurities.

CONCLUSIONS

Enrichment of high aspect ratio SWNTs was obtained via a readily scalable batch purification method. The sedimentation method of centrifugation that was used in these studies differs from density gradient ultracentrifugation in that the addition of solutes to form zones of varying gradients in the solvent are not needed. This allowed the purification and enrichment process to occur without the addition of additional reagents, many of which are difficult to remove in subsequent steps. The buoyancy of surfactant-encapsulated SWNTs increased with length. Then, the low centripetal forces used in these studies not only removed low aspect ratio SWNTs and impurities but also allowed the enhanced buoyancy of unbundled high aspect ratio surfactant-encapsulated SWNTs to be used to isolate them in the supernatant. For all processing conditions, an increase in the purity deposits, relative to the suspensions, was observed via Raman spectroscopy. This indicates that the reduced translational diffusion coefficient of high aspect ratio SWNTs promotes their deposition over residual low aspect ratio impurities and nanotubes.

AUTHOR INFORMATION

Corresponding Author
mlay@uga.edu
Notes
The authors declare no competing financial interest.

ACKNOWLEDGMENTS

REFERENCES

(1) Ruoff, R. S.; Yu, M.-F.; Rohrs, H. *Nanomanipulation and Characterization of Individual Carbon Nanotubes Recent Advances in Experimental Mechanics*; Gdoutos, E. E., Ed.; Springer: Netherlands, 2004; pp 65−74.
(2) Bocharova, V.; Kiriy, A.; Oertel, U.; Stamm, M.; Stoffelbach, F.; Jerome, R.; Detrembleur, C. *J. Phys. Chem. B* **2006**, *110*, 14640.
(3) Hu, L.; Hecht, D. S.; Gruner, G. *Nano Lett.* **2004**, *4*, 2513.
(4) Durkop, T.; Getty, S. A.; Cobas, E.; Fuhrer, M. S. *Nano Lett.* **2004**, *4*, 35.
(5) Nakamura, S.; Ohishi, M.; Shiraishi, M.; Takenobu, T.; Iwasa, Y. *Appl. Phys. Lett.* **2006**, *89*, 013112.
(6) Bradley, K.; Gabriel, J. C. P.; Gruner, G. *Nano Lett.* **2003**, *3*, 1353.
(7) Wildoer, J. W. G.; Venema, L. C.; Rinzler, A. G.; Smalley, R. E.; Dekker, C. *Nature* **1998**, *391*, 59.
(8) Weber, J.; Kumar, A.; Kumar, A.; Bhansali, S. *Sens. Actuators, B* **2006**, *117*, 308.
(9) Kwon, J.-H.; Lee, K.-S.; Lee, Y.-H.; Ju, B.-K. *Electrochem. Solid-State Lett.* **2006**, *9*, H85.
(10) Pengfei, Q. F.; Vermesh, O.; Grecu, M.; Javey, A.; Wang, O.; Dai, H. J.; Peng, S.; Cho, K. J. *Nano Lett.* **2003**, *3*, 347.
(11) Patra, S. K.; Rao, G. M. *J. Appl. Phys.* **2006**, *100*, 024319.
(12) Wang, M. S.; Peng, L. M.; Wang, J. Y.; Jin, C. H.; Chen, Q. *J. Phys. Chem. B* **2006**, *110*, 9397.
(13) Newson, R. W.; Green, A. A.; Hersam, M. C.; van Driel, H. M. *Phys. Rev. B* **2011**, *83*, 115421.
(14) Li, E. Y.; Marzari, N. *ACS Nano* **2011**, *5*, 9726.
(15) Javey, A.; Guo, J.; Wang, Q.; Lundstrom, M.; Dai, H. J. *Nature* **2003**, *424*, 654.
(16) Zhao, J.; Lin, C.; Zhang, W.; Xu, Y.; Lee, C. W.; Chan-Park, M. B.; Chen, P.; Li, L.-J. *J. Phys. Chem. C* **2011**, *115*, 6975.
(17) Sarker, B. K.; Shekhar, S.; Khondaker, S. I. *ACS Nano* **2011**, *5*, 6297.
(18) Engel, M.; Small, J. P.; Steiner, M.; Freitag, M.; Green, A. A.; Hersam, M. C.; Avouris, P. *ACS Nano* **2008**, *2*, 2445.
(19) Cheon, J. H.; Bae, J. H.; Jang, J. *Solid-State Electron.* **2008**, *52*, 473.
(20) Gleskova, H.; Hsu, P. I.; Xi, Z.; Sturm, J. C.; Suo, Z.; Wagner, S. *J. Non-Cryst. Solids* **2004**, *338*, 732.
(21) Schmidt, J. A.; Hundhausen, M.; Ley, L. *Phys. Rev. B* **2001**, *64*, 104201.
(22) Sato, S.; Seki, S.; Honsho, Y.; Wang, L.; Nikawa, H.; Luo, G.; Lu, J.; Haranaka, M.; Tsuchiya, T.; Nagase, S.; Akasaka, T. *J. Am. Chem. Soc.* **2011**, *133*, 2766.
(23) Heremans, P.; Cheyns, D.; Rand, B. P. *Acc. Chem. Res.* **2009**, *42*, 1740.
(24) Rouhi, N.; Jain, D.; Burke, P. J. *ACS Nano* **2011**, *5*, 8471.
(25) Jeong, H. J.; Jeong, H. D.; Kim, H. Y.; Kim, J. S.; Jeong, S. Y.; Han, J. T.; Bang, D. S.; Lee, G. W. *Adv. Funct. Mater.* **2011**, *21*, 1526.
(26) Kim, S.; Park, J.; Ju, S.; Mohammadi, S. *ACS Nano* **2010**, *4*, 2994.
(27) Jiao, L. Y.; Xian, X. J.; Wu, Z. Y.; Zhang, J.; Liu, Z. F. *Nano Lett.* **2009**, *9*, 205.
(28) Gonzalez-Dominguez, J. M.; Gonzalez, M.; Anson-Casaos, A.; Diez-Pascual, A. M.; Gomez, M. A.; Martinez, M. T. *J. Phys. Chem. C* **2011**, *115*, 7238.
(29) Shim, B. S.; Zhu, J.; Jan, E.; Critchley, K.; Ho, S.; Podsiadlo, P.; Sun, K.; Kotov, N. A. *ACS Nano* **2009**, *3*, 1711.
(30) Porro, S.; Musso, S.; Vinante, M.; Vanzetti, L.; Anderle, M.; Trotta, F.; Tagliaferro, A. *Physica E* **2007**, *37*, 58.
(31) Holzinger, M.; Hirsch, A.; Bernier, P.; Duesberg, G. S.; Burghard, M. *Appl. Phys. A* **2000**, *70*, 599.
(32) Li, J. X.; Chajara, K.; Lindgren, J.; Grennberg, H. *J. Nanosci. Nanotechnol.* **2007**, *7*, 1525.
(33) Worsley, K. A.; Kalinina, I.; Bekyarova, E.; Haddon, R. C. *J. Am. Chem. Soc.* **2009**, *131*, 18153.
(34) Hersam, M. C. *Nat. Nanotechnol.* **2008**, *3*, 387.
(35) Tabakman, S. M.; Welsher, K.; Hong, G.; Dai, H. *J. Phys. Chem. C* **2010**, *114*, 19569.
(36) Carvalho, E. J. F.; dos Santos, M. C. *ACS Nano* **2010**, *4*, 765.
(37) Ghosh, S.; Bachilo, S. M.; Weisman, R. B. *Nat. Nanotechnol.* **2010**, *5*, 443.
(38) Yi, W.; Malkovskiy, A.; Chu, Q.; Sokolov, A. P.; Colon, M. L.; Meador, M.; Pang, Y. *J. Phys. Chem. B* **2008**, *112*, 12263.
(39) Vichchulada, P.; Shim, J.; Lay, M. D. *J. Phys. Chem. C* **2008**, *112*, 19186.

9360

dx.doi.org/10.1021/ja302136x | *J. Am. Chem. Soc.* 2012, 134, 9352−9361

(40) Vairavapandian, D.; Vichchulada, P.; Lay, M. D. *Anal. Chim. Acta* **2008**, *626*, 119.

(41) Shim, J.; Vichchulada, P.; Zhang, Q.; Lay, M. D. *J. Phys. Chem. C* **2010**, *114*, 652.

(42) Carvalho, E. J. F.; dos Santos, M. C. *ACS Nano* **2010**, *4*, 765.

(43) Valcarcel, M.; Cardenas, S.; Simonet, B. M. *Anal. Chem.* **2007**, *79*, 4788.

(44) Zhang, Q.; Vichchulada, P.; Shivareddy, S. B.; Lay, M. D. *J. Mater. Sci.* **2012**, *47*, 6812.

(45) Zhang, Q.; Vichchulada, P.; Lay, M. D. *J. Phys. Chem. C* **2010**, *114*, 16292.

(46) Vichchulada, P.; Zhang, Q.; Duncan, A.; Lay, M. D. *ACS Appl. Mater. Interfaces* **2010**, *2*, 467.

(47) Zhang, Q.; Vichchulada, P.; Cauble, M. A.; Lay, M. D. *J. Mater. Sci.* **2009**, *44*, 1206.

(48) Zhu, J.; Shim, B. S.; Di Prima, M.; Kotov, N. A. *J. Am. Chem. Soc.* **2011**, *133*, 7450.

(49) Jaber-Ansari, L.; Hahm, M. G.; Somu, S.; Sanz, Y. E.; Busnaina, A.; Jung, Y. J. *J. Am. Chem. Soc.* **2009**, *131*, 804.

(50) Jang, E. Y.; Kang, T. J.; Im, H. W.; Kim, D. W.; Kim, Y. H. *Small* **2008**, *4*, 2255.

(51) Vichchulada, P.; Cauble, M. A.; Abdi, E. A.; Obi, E. I.; Zhang, Q.; Lay, M. D. *J. Phys. Chem. C* **2010**, *114*, 12490.

(52) Chow, B. Y.; Mosley, D. W.; Jacobson, J. M. *Langmuir* **2005**, *21*, 4782.

(53) Priya, B. R.; Byrne, H. J. *J. Phys. Chem. C* **2008**, *112*, 332.

(54) Rance, G. A.; Marsh, D. H.; Nicholas, R. J.; Khlobystov, A. N. *Chem. Phys. Lett.* **2010**, *493*, 19.

(55) Horcas, I.; Fernandez, R.; Gomez-Rodriguez, J. M.; Colchero, J.; Gomez-Herrero, J.; Baro, A. M. *Rev. Sci. Instrum.* **2007**, *78*, 013705.

(56) Ryabenko, A. G.; Dorofeeva, T. V.; Zvereva, G. I. *Carbon* **2004**, *42*, 1523.

(57) Hare, J. P.; Kroto, H. W.; Taylor, R. *Chem. Phys. Lett.* **1991**, *177*, 394.

(58) Bachilo, S. M.; Strano, M. S.; Kittrell, C.; Hauge, R. H.; Smalley, R. E.; Weisman, R. B. *Science* **2002**, *298*, 2361.

(59) Tsyboulski, D. A.; Bachilo, S. M.; Kolomeisky, A. B.; Weisman, R. B. *ACS Nano* **2008**, *2*, 1770.

(60) Arnold, M. S.; Green, A. A.; Hulvat, J. F.; Stupp, S. I.; Hersam, M. C. *Nat. Nanotechnol.* **2006**, *1*, 60.

(61) Kavan, L.; Frank, O.; Green, A. A.; Hersam, M. C.; Koltai, J. n.; Zólyomi, V.; Kürti, J.; Dunsch, L. *J. Phys. Chem. C* **2008**, *112*, 14179.

(62) Nair, N.; Kim, W.-J.; Braatz, R. D.; Strano, M. S. *Langmuir* **2008**, *24*, 1790.

(63) Duque, J. G.; Densmore, C. G.; Doorn, S. K. *J. Am. Chem. Soc.* **2010**, *132*, 16165.